EUROPEAN ORGANIZATION FOR NUCLEAR RESEARCH

DIRAC Note 2012-07
October 21, 2012

Amplitude alignment for preshower detector

M.Pentia, J.Smolik, V.Yazkov

GENEVA
2012

Abstract

The Preshower detector together with the Cherenkov Nitrogen detector are used for electron-positron background rejection using amplitude information. In the present work, the Preshower signal amplitudes are corrected for the light attenuation and inhomogeneity of individual Preshower scintillator slabs

1. Introduction

The main task of the Preshower (PSh) detector [1] for DIRAC-II experiment is rejection of the large electron-positron background. The detector consists of 40 scintillation slabs, placed symmetrically along the two arms, for positive and negative particles.

In the high energy phase space region of the kaon flight, the PSh detector has two layers, to reject for the pion contamination due to Nitrogen Cherenkov detector.

The PSh geometrical characteristics are presented in **Figure 1.** It contains, in the first layer a *Pb* converter of 10*mm* thickness for the first two slabs and 25*mm* for the rest. The second layer is placed behind the first one, in the kaon flight region. It contains a *Pb* converter of 10*mm* thickness. The detector slabs, placed behind the *Pb* converter, are plastic scintillators BICRON type 408 of 10*mm* thickness.

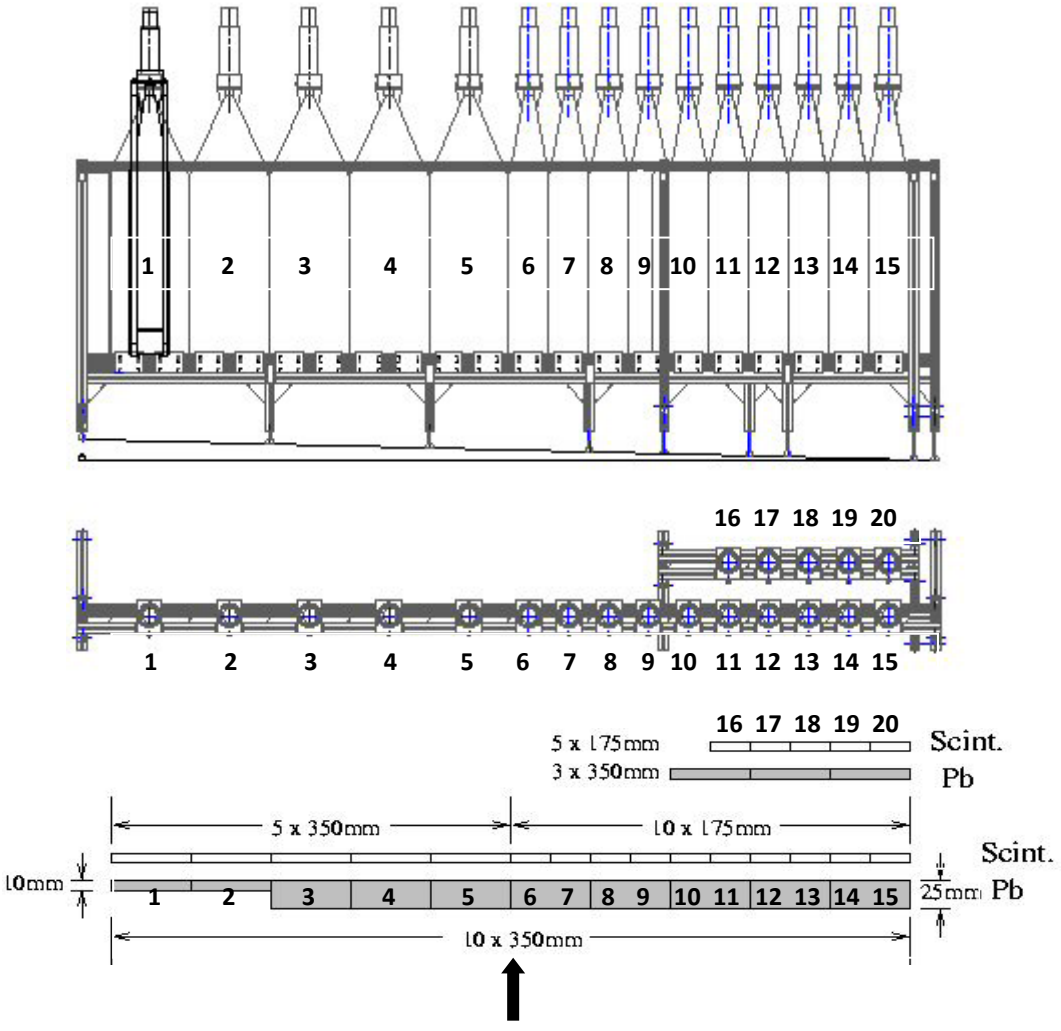

Figure 1. The preshower left arm geometry and structure.

Each scintillation slab provides detection of the particles after *Pb* converter. The signal produced by a high energy pion has a low amplitude, because it losses energy mainly by direct ionization as m.i.p.'s. So the amplitude (ADC) spectrum shows a sharp peak around a low mean value (see **Figure 2.a**) and a higher amplitude tail due to shower particles produced in *Pb* by some of the pions. The tail contribution increases with the pion energy.

On the other hand, a relativistic electron incident on *Pb* converter, produces an electromagnetic shower of electrons and photons. In interaction with the scintillation material they produce a large amplitude signal, proportional to the total absorbed energy. Therefore, the amplitude spectrum of high energy electrons shows a broad distribution (see **Figure 2. b**) centered around a high amplitude mean value.

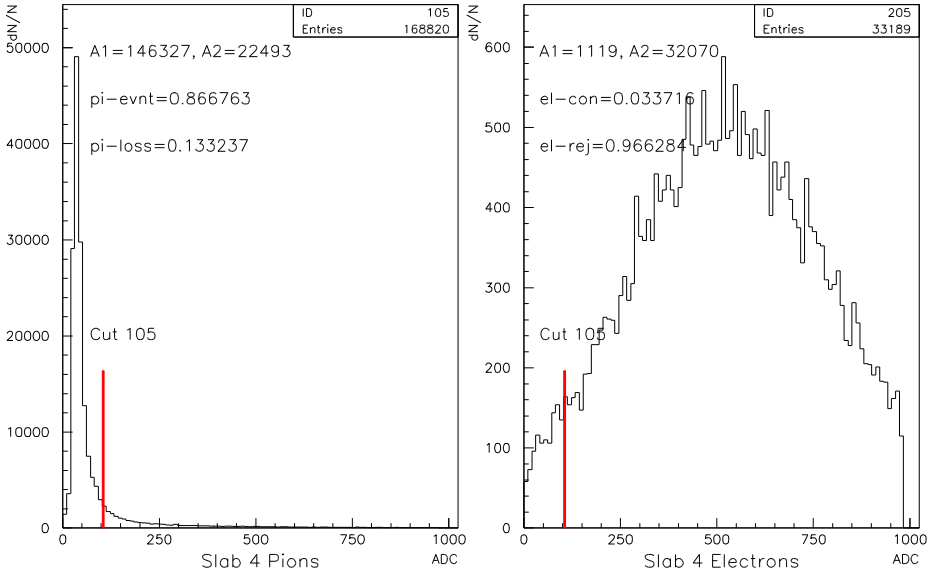

a. Raw pion amplitude distribution **b.** Raw electron amplitude distribution

Figure 2. The typical PSh amplitude spectra for pions and electrons detected in PSh slab 4 negative arm, in anticoincidence, respective coincidence with the Nitrogen Cherenkov detector signals. The *e-π* cut channel separation is placed between the pion and electron amplitude distribution spectra.

In general the PSh amplitude signal depends on some parameters, as:

- Particle type
- Momentum of detected particles
- Coordinates of the particle hit on PSh slab
- Amplification inhomogeneities in each channel

The aim of this work is to apply corrections on the amplitude as to eliminate the last two dependencies and so, the remaining two dependencies can be used to identify and separate particles and even evaluate their momentum.

The amplitude distribution of the m.i.p. (pions and muons) signal, does not depend on particle momentum. Therefore it is very convenient to use the pion peak position to study the response dependence on the hit coordinates (x,y) of the Preshower slabs. So the amplitude will be function just on the light attenuation degree in the scintillator material.

2. Amplitude dependence on particle hit position

The large dimensions of the PSh scintillators (see **Figure 4**) imply a relatively long light path (see **Figure 5**) to the photomultiplier photocathode. So, the scintillation light is more or less attenuated, depending on the scintillation original point, detected particle incidence point. Correspondingly, the signal amplitude is a function on the coordinate (*x*,*y*) of this point. The simulated amplitude dependence on hit position is shown in **Figure 6**.

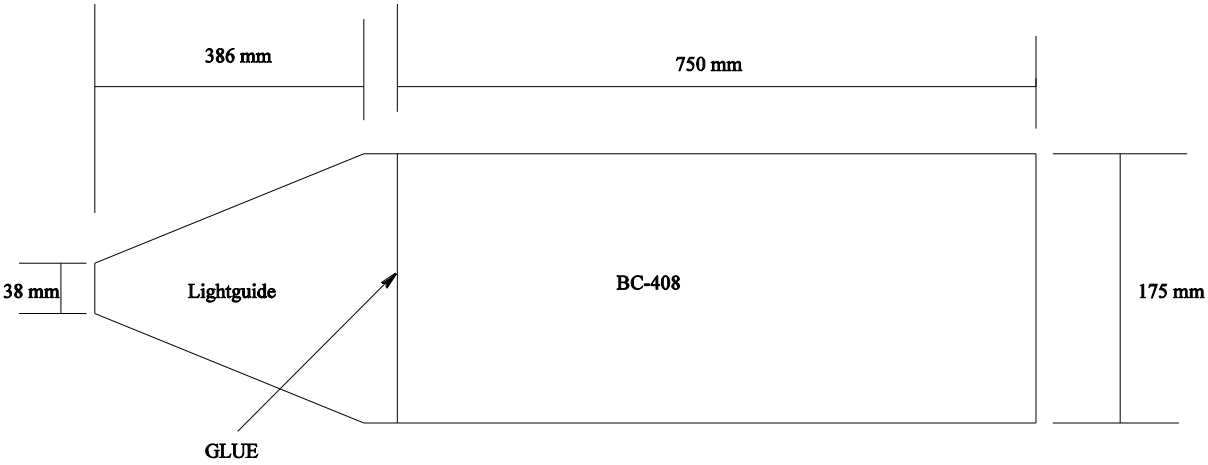

Figure 4. Preshower slab geometry for the small scintillators (6-15)

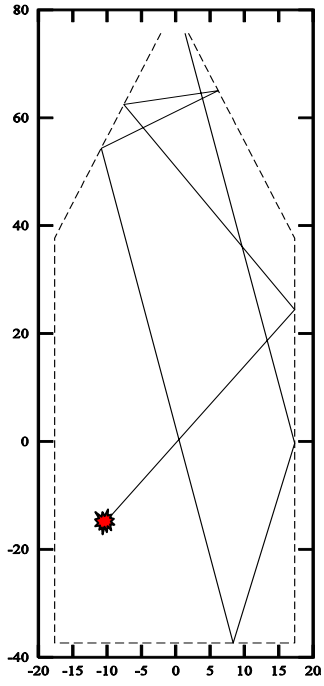

Figure 5. Simulation of a light track in a large scintillator slab (arbitrary units)

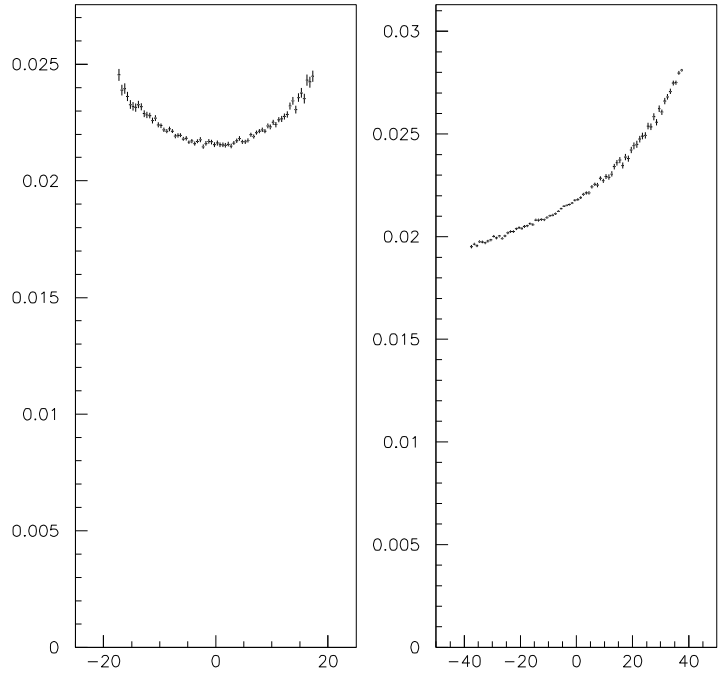

a. **b.**

Figure 6. The simulation of the output light yield from a large scintillator slab as a function of *x* (**Fig. 6.a**) and *y* (**Fig. 6.b**) coordinates of the particle incidence (arbitrary units).

3. The raw pion amplitude analysis

The DIRAC data taking has been done in different conditions, and lasts for a long time (about 5-6 months per year). These imply possible fluctuations in the pion peak position, for different runs. Also, the pion peak position is different from one slab to another one along all 40 slabs, and even for the same slab, from one incident point (*x*,*y*) to another one.

Our aim is to correct for these fluctuations and to obtain the alignment for all pion peak positions to the same amplitude value for all runs and for all slabs.

3.1 Pedestal and Cut corrections for the raw data

The data taking has been done with the „cut" subtraction and „pedestal" addition. So to reconstruct the amplitude distribution it is necessary to do the corresponding correction by add the „cut" and subtract „pedestal" values for each slab. So the first raw data amplitude corrections are presented in **Figure 7**, as an example for run 11999, slab (1,1,4) (arm, plane, slab).

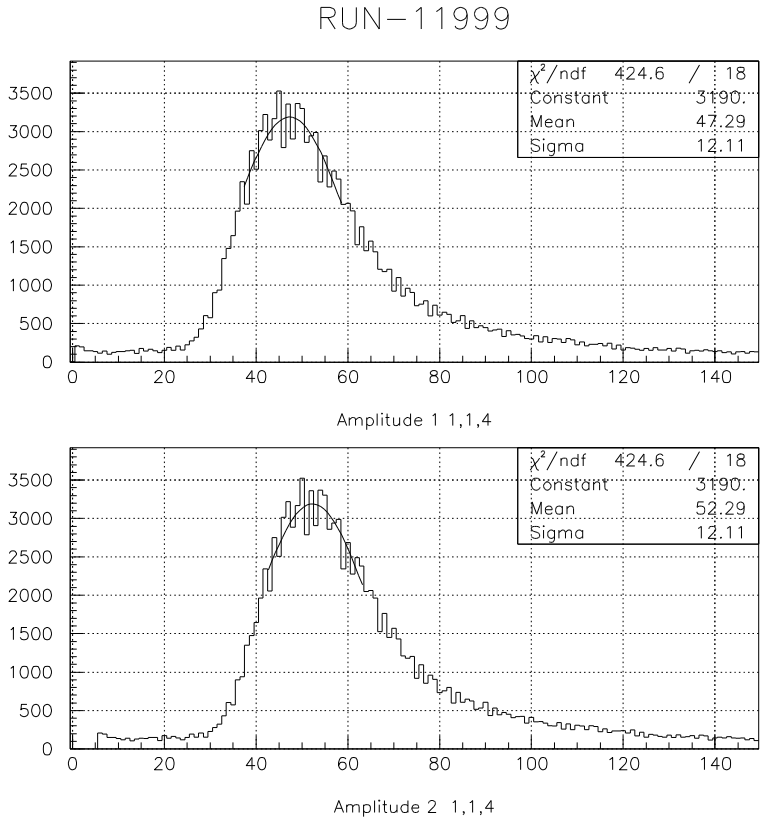

Figure 7. Raw pion amplitude distribution before (up) and after (down) +cut and -ped corrections for PSh arm-1, plane-1, slab-4 (1,1,4), Run 11999.

These corrections were done for all 2008 runs 7822-8603, for 2009 runs 8605-9820, for 2010 runs 9821-11246, for 2011 runs 11256-12308, and for all 40 channels of the PSh.

3.2 The reference run interval selection

All raw pion amplitude distributions have been fitted with a Gaussian to find the mean amplitude position for all 40 slabs and for all runs of a year (see **Figure 8**). Then the collection of all peak positions for all runs of one year was plotted to find a reference interval of runs with stable peak positions (see **Figure 9** for 2011 reference run interval).

The reference amplitude values are used for determination of the (x,y)-dependence for each slab.

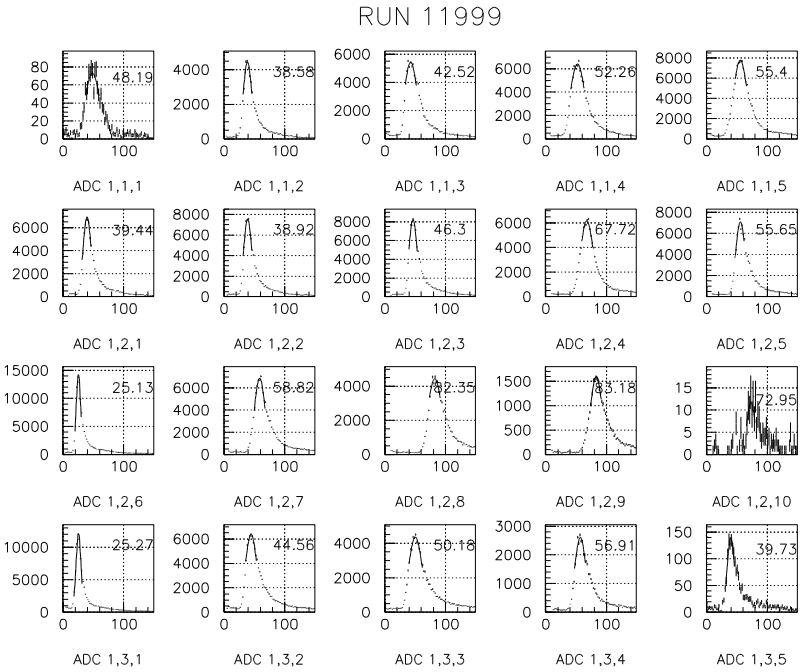

Figure 8. Gaussian fit of the raw pion peak position for slabs Arm 1, Run 11999.

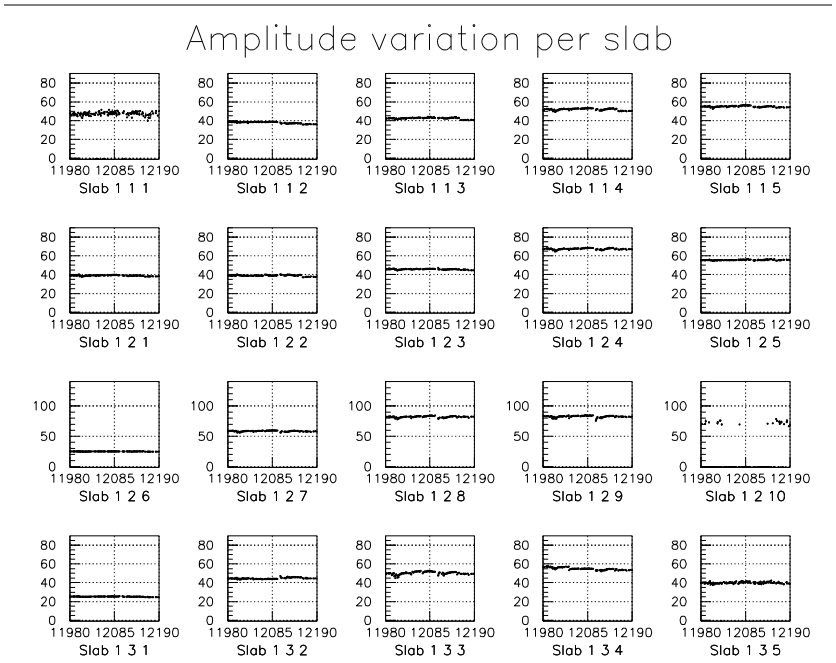

Figure 9. The 2011 reference runs for raw pion peak position versus run number for slabs Arm 1

4. The (*x*,*y*) dependence of the raw pion amplitude for individual slabs

All pion amplitude values from reference runs are put together and plotted versus *x*- and *y*-coordinate for each slab (see **Figure 10**). The dependence behavior corresponds to the simulated one, see **Figure 6a, b**. The *x*- and *y*-dependences are treated as mutually independent.

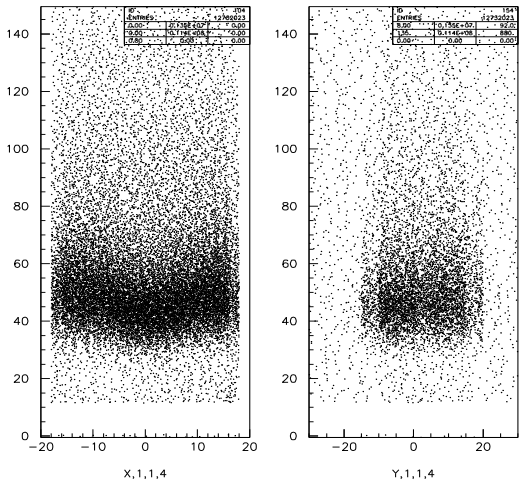

Figure 10. Scatter plot of the raw pion amplitude versus *x*- and *y*-coordinate for the slab (1,1,4) and for all reference runs (11980 – 12190). On *x*-dependence the clear deep is visible in middle of the slab

4.1 The *x*-dependence of the raw pion amplitude

To obtain and describe the *x*-dependence of the raw pion amplitude, each slab has been divided into 2*cm* slices: 20 slices along *x*-axis for slabs (1-5) plane 1, and 10 slices for slabs (6-20) plane 2 and 3. The pion peak has been fitted for each slice (see **Figure 11**) to obtain the *x*-dependence of the raw pion amplitude (see **Figure 12**) for all slabs.

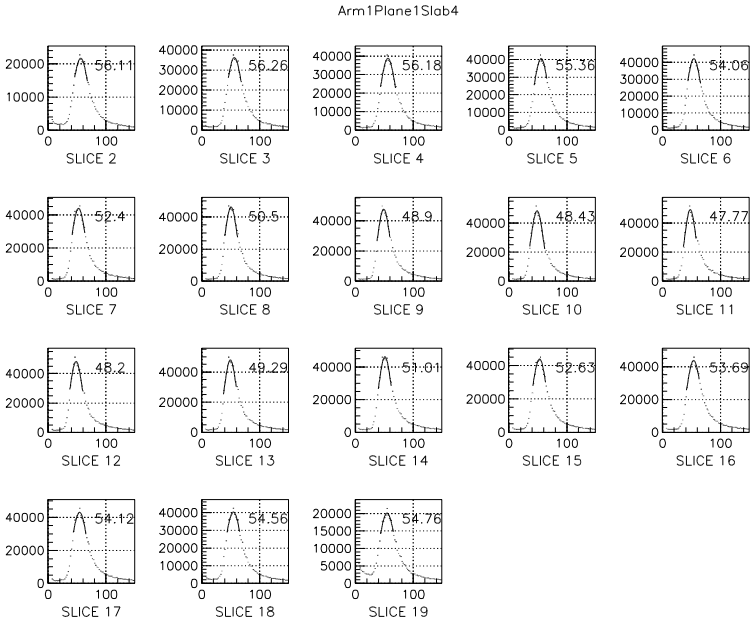

Figure 11. Gaussian fit for raw pion amplitude distribution for the 10 *x*-slices of the (1,1,4) slab.

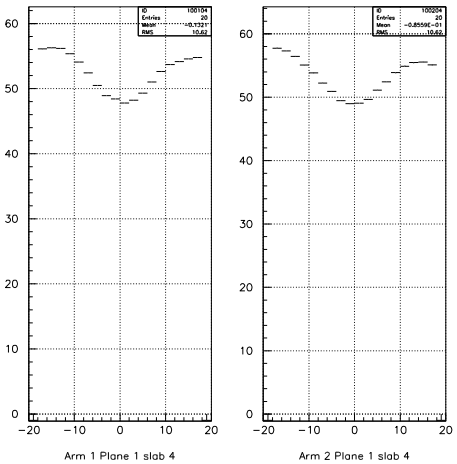

Figure 12. *x*-dependence of the raw pion amplitude for two slabs: (1,1,4) and (2,1,4).

The final *x*-dependence has been fitted with a linear + Gaussian function:

$$A_{(x)}^{fit} = a_x + b_x x + c_x e^{-\frac{(x-d_x)^2}{2\sigma^2}} \quad (1)$$

In **Figure 13** the fit for two slabs is presented. The parameters match: $a_x \equiv$ P1, $b_x \equiv$ P2, $c_x \equiv$ P3, $d_x \equiv$ P4, $\sigma \equiv$ P5. In **Figure 13** the slab (1,1,1) is not fully covered by particle tracks over *x* coordinate.

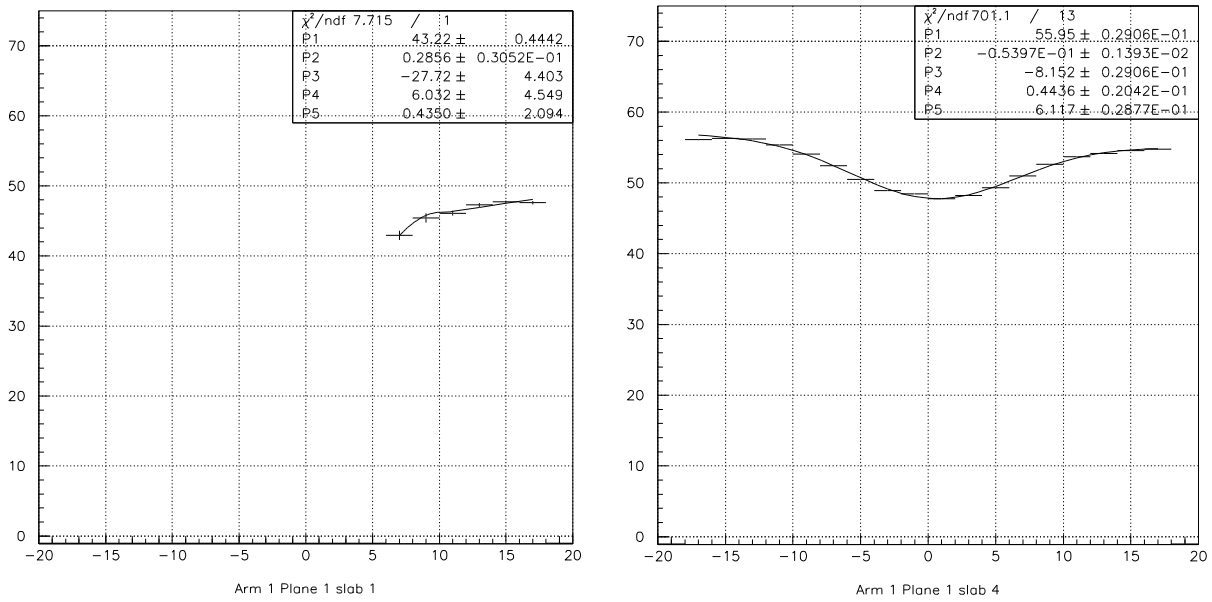

Figure 13. Linear + Gaussian fit *x*-dependence of the raw pion peak position for two slabs (1,1,1) and (1,1,4) with the corresponding fit parameters.

TABLE 1. The *x*-dependence fit parameters of the raw pion amplitude for all 40 slabs of the PSh.

Slab	P1	P2	P3	P4	P5	Slab	P1	P2	P3	P4	P5
1 1 1	43.2250	0.2856	-27.7210	6.0319	0.4350	2 1 1	71.8106	0.0701	-6.0596	-7.3973	0.8320
1 1 2	40.4500	-0.0391	-4.8335	-0.3495	6.3430	2 1 2	48.1630	-0.3703	-9.3374	0.4411	5.9690
1 1 3	45.3905	0.0915	-6.6464	-0.4621	4.9399	2 1 3	56.7398	-0.1221	-9.4012	0.0497	5.9326
1 1 4	55.9554	-0.0540	-8.1529	0.4437	6.1181	2 1 4	56.9943	-0.0633	-8.1779	-0.7039	6.5328
1 1 5	58.6095	-0.0093	-7.9350	-0.0052	6.3339	2 1 5	34.0734	-0.0177	-2.6225	-0.5557	5.4910
1 2 1	40.1487	-0.0646	-1.8330	-2.1774	4.5296	2 2 1	42.1689	-0.0242	-2.9616	-0.1350	5.5660
1 2 2	40.2840	-0.0872	-1.9269	-0.7106	4.7574	2 2 2	35.6657	0.0150	-1.2587	-0.8527	4.3400
1 2 3	46.8395	0.0000	-1.7446	-1.4049	3.7469	2 2 3	42.6087	0.0206	-2.7060	-1.0945	4.5519
1 2 4	69.6828	-0.1031	-3.6137	-0.2524	4.0734	2 2 4	46.4738	-0.0022	-3.1262	-1.8361	4.1701
1 2 5	58.6700	-0.0335	-3.9354	-0.3465	5.7822	2 2 5	40.3240	0.0526	-1.8226	-1.7107	4.7417
1 2 6	28.0886	-0.1703	-3.4108	-6.6524	11.6760	2 2 6	54.4346	-0.1027	-2.4973	-1.0811	4.3439
1 2 7	60.3356	-0.0089	-2.5622	-11.0363	4.0118	2 2 7	38.2844	0.0701	-2.9930	-0.5538	5.7278
1 2 8	83.4463	-0.0351	-1.6957	-0.5420	3.4369	2 2 8	33.9267	0.0090	-1.0170	0.5015	4.6215
1 2 9	84.4870	0.0429	-2.1288	-0.0626	4.8800	2 2 9	54.7578	-0.0507	-2.1647	-0.4245	4.7766
1 2 10	74.0306	0.0570	-7.7726	0.4736	3.3890	2 2 10	83.5032	0.4122	-9.7444	7.3753	2.8917
1 3 1	25.6940	0.0132	-0.8324	-1.4567	4.4156	2 3 1	37.4298	-0.0605	-1.8041	0.7902	4.5199
1 3 2	47.2963	0.1176	-3.3695	-2.1103	4.4945	2 3 2	57.4088	-0.0055	-4.0727	0.5222	5.0764
1 3 3	52.3404	0.0553	-2.9186	-0.6608	4.3784	2 3 3	79.3956	0.1571	-4.5575	-0.1865	4.8647
1 3 4	56.2718	0.0110	-2.2436	0.0804	3.0651	2 3 4	51.5138	-0.0345	-4.4148	-0.1392	3.8330
1 3 5	41.9740	-1.0912	-11.5233	-10.9277	6.8026	2 3 5	72.2605	0.3008	-2.1999	3.0955	6.5973

4.2 The *x*-correction of the raw pion amplitude

To eliminate the *x*-dependence of the raw amplitude fit function (1) we must have only $a_x \neq 0$. Therefore, the correction coefficient δ_x (see **Figure 14** with $a_x \equiv$P1), is:

$$\delta_{(x)} = \frac{a_x}{A^{fit}_{(x)}} \qquad (2)$$

and the <u>*x*-corrected amplitude</u> $A^{cor}_{(x)}$ is:

$$A^{cor}_{(x)} = \delta_{(x)} A^{raw}_{(x,y)} = \frac{a_x}{A^{fit}_{(x)}} A^{raw}_{(x,y)} \qquad (3)$$

For example, if the <u>raw data</u> amplitude $A^{raw}_{(x,y)} = A^{fit}_{(x)}$, the <u>*x*-corrected amplitude</u> is the constant $A^{cor}_{(x)} = a_x$.

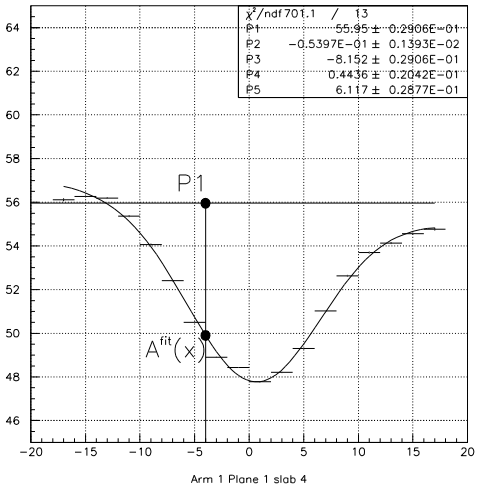

Figure 14. The *x*-dependence correction for slab (1,1,4).

4.3 The *x*-corrected pion amplitude spectra

We applied (3) to *x*-correct the raw amplitude data $A^{raw}_{(x,y)}$ for all slabs and runs, both for *x*- and *y*-dependence. So the raw amplitudes $A^{raw}_{(x,y)}$ as in **Figure 10**, were *x*-corrected, and now they are $A^{cor}_{(x)}$ as in **Figure 15**.

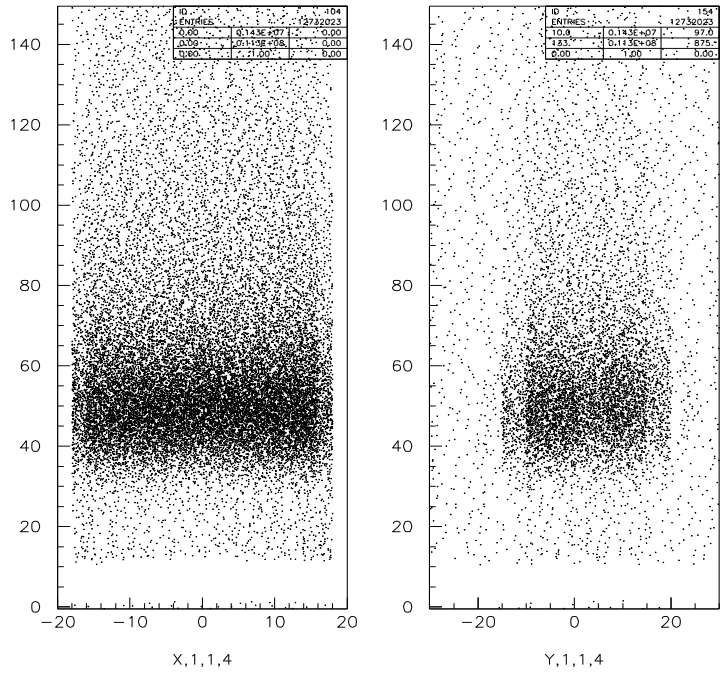

Figure 15. <u>*x*-corrected amplitude</u> for *x*- and *y*-distribution for all runs, slab (1,1,4). To be compared with the **Figure 10** <u>raw pion amplitude.</u> Here are no more central deep on *x*-distribution.

We must to continue with the amplitude *y*-correction.

4.4 The *y*-dependence of the *x*-corrected pion amplitude

With the obtained *x*-corrected amplitude we proceed to obtain and describe the *y*-dependence of the amplitude. So, each slab has been divided into 12 slices along to *y*-coordinate. The pion peak has been fitted for each slice (see **Figure 16**) and have been obtained the *y*-dependence of the *x*-corrected amplitude (see **Figure 17**) for all slabs.

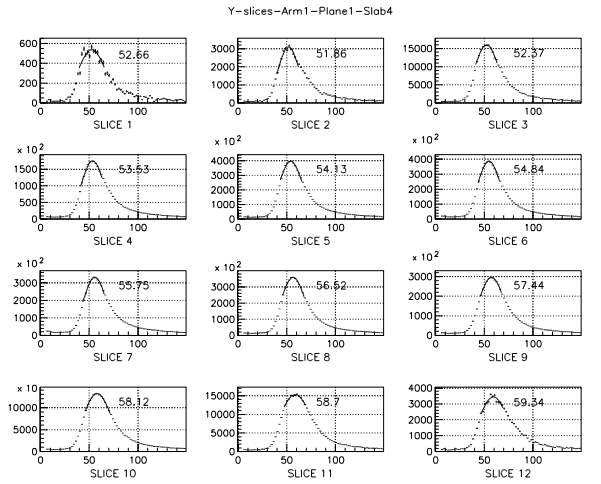

Figure 16. Gaussian fit of *x*-corrected amplitude for the 12 *y*-slices of the (1,1,4) slab.

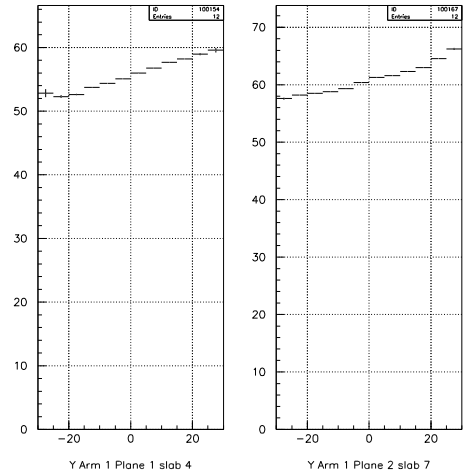

Figure 17. *y*-dependence of the *x*-corrected amplitude for slab (1,1,4) and (1,2,7).

The *y*-dependence of the *x*-corrected amplitude has been fitted with a polynomial function:

$$A_{(y)}^{fit} = a_y + b_y y + c_y y^2 + d_y y^3 + e_y y^4 \qquad (4)$$

In **Figure 18** it is presented the fit for slab (1,1,4). The parameters a_y≡P1, b_y≡P2, c_y≡P3, d_y≡P4, e_y≡P5

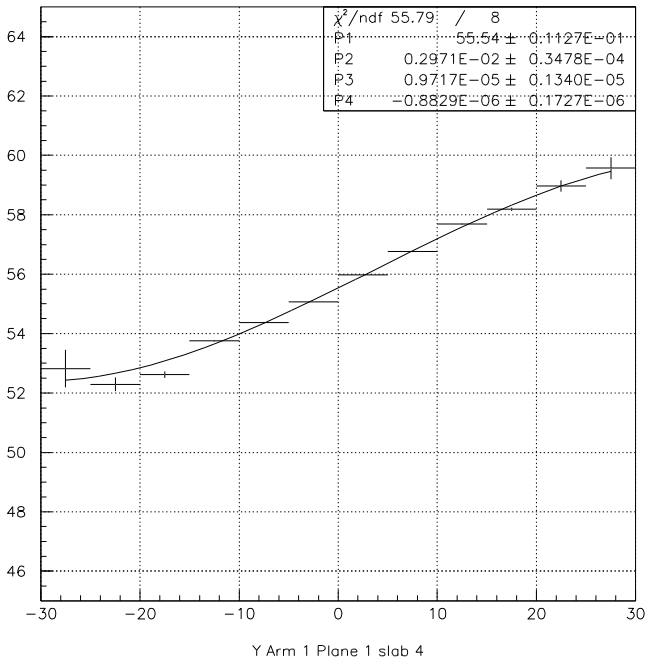

Figure 18. Polynomial fit *y*-dependence of the *x*-corrected amplitude for slab (1,1,4) with the corresponding fit parameters of a third degree polynomial.

TABLE 2. The *y*-dependence fit parameters of the *x*-corrected amplitude for all 40 slabs of the Preshower detector.

Slab	P1	P2	P3	P4	P5
1 1 1	41.2128	0.913E-02	0.780E-04	-0.655E-05	0.000E+00
1 1 2	40.4177	0.974E-03	-0.658E-04	0.305E-05	0.000E+00
1 1 3	45.2130	0.279E-02	0.269E-04	-0.543E-06	-0.250E-07
1 1 4	55.5381	0.297E-02	0.974E-05	-0.883E-06	0.000E+00
1 1 5	58.2851	0.165E-02	0.295E-04	0.711E-06	0.000E+00
1 2 1	40.2923	0.131E-02	-0.171E-04	0.931E-06	0.000E+00
1 2 2	40.2577	0.224E-02	0.474E-05	0.000E+00	0.000E+00
1 2 3	46.7173	0.135E-02	0.779E-05	0.000E+00	0.000E+00
1 2 4	69.7799	0.161E-02	-0.820E-05	0.000E+00	0.000E+00
1 2 5	59.0054	0.191E-02	0.177E-04	0.000E+00	0.000E+00
1 2 6	27.5519	0.528E-03	0.407E-05	0.000E+00	0.000E+00
1 2 7	60.4878	0.228E-02	0.214E-04	0.000E+00	0.000E+00
1 2 8	83.9656	0.127E-02	-0.162E-04	0.000E+00	0.000E+00
1 2 9	84.5368	0.113E-02	0.122E-04	0.000E+00	0.000E+00
1 2 10	72.9463	0.263E-02	0.760E-04	0.000E+00	0.000E+00
1 3 1	25.6940	0.221E-02	0.219E-04	-0.248E-07	0.000E+00
1 3 2	47.2713	0.335E-02	0.276E-04	-0.181E-05	0.000E+00
1 3 3	52.5033	0.264E-02	0.154E-04	0.000E+00	0.000E+00
1 3 4	56.3543	0.107E-02	0.247E-04	0.000E+00	0.000E+00
1 3 5	42.8108	0.385E-02	0.628E-04	-0.800E-06	0.000E+00

Slab	P1	P2	P3	P4	P5
2 1 1	69.4497	0.495E-02	0.266E-03	0.988E-05	0.000E+00
2 1 2	47.2882	0.364E-02	-0.122E-03	0.523E-05	0.606E-06
2 1 3	55.9213	0.146E-02	0.548E-04	0.439E-05	0.897E-07
2 1 4	56.3581	0.178E-02	0.627E-04	0.171E-05	0.000E+00
2 1 5	34.1059	0.124E-02	-0.254E-04	-0.169E-06	0.622E-07
2 2 1	41.8914	0.107E-02	0.271E-04	0.409E-06	0.000E+00
2 2 2	35.4738	0.142E-02	0.260E-04	0.936E-06	0.000E+00
2 2 3	42.4051	0.294E-02	0.290E-04	-0.747E-06	0.000E+00
2 2 4	46.3212	0.192E-02	0.386E-04	0.000E+00	0.000E+00
2 2 5	40.1910	0.174E-02	0.130E-04	0.000E+00	0.000E+00
2 2 6	54.3371	0.371E-03	0.120E-04	0.000E+00	0.000E+00
2 2 7	38.3555	0.191E-02	0.915E-05	0.000E+00	0.000E+00
2 2 8	33.8539	0.257E-02	0.190E-04	0.103E-05	0.957E-07
2 2 9	54.8603	0.641E-03	0.121E-04	0.000E+00	0.000E+00
2 2 10	80.0195	0.237E-02	0.902E-04	0.000E+00	0.000E+00
2 3 1	37.4048	0.424E-03	0.663E-06	0.000E+00	0.000E+00
2 3 2	57.0746	0.140E-02	0.408E-04	0.000E+00	0.000E+00
2 3 3	79.4901	0.186E-02	-0.130E-05	-0.112E-05	0.000E+00
2 3 4	51.8217	0.107E-02	0.262E-04	0.925E-06	0.000E+00
2 3 5	72.1169	0.160E-02	0.279E-04	0.000E+00	0.000E+00

4.5 *y*-correction of the pion amplitude

To eliminate the *y*-dependence in the amplitude relation (4) we must have only $a_y \neq 0$. Therefore, the *y*-correction coefficient $\delta_{(y)}$ (see **Figure 19**, with $a_y \equiv$P1), is:

$$\delta_{(y)} = \frac{a_y}{A^{fit}_{(y)}} \tag{5}$$

and the *y*-corrected amplitude $A^{cor}_{(y)}$, is:

$$A^{cor}_{(y)} = \delta_{(y)} A^{raw}_{(x,y)} = \frac{a_y}{A^{fit}_{(y)}} A^{raw}_{(x,y)} \tag{6}$$

For example, if the raw data amplitude $A^{raw}_{(x,y)} = A^{fit}_{(y)}$, the corrected amplitude is the constant $A^{cor}_{(y)} = a_y$.

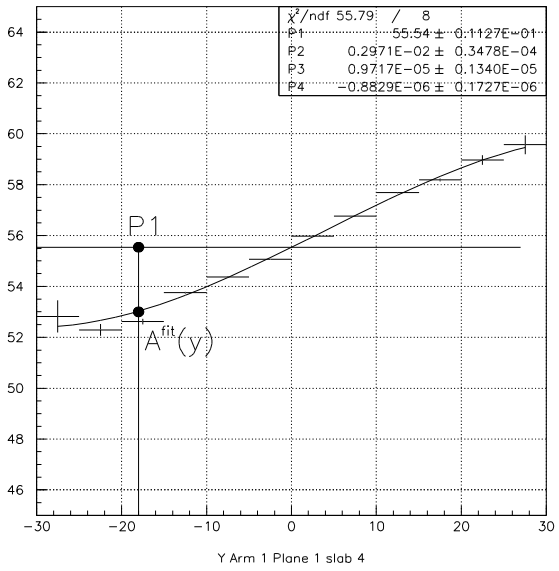

Figure 19. The *y*-dependence correction for slab (1,1,4).

4.6 Combined *xy*-correction of the raw pion amplitude

The *x*- and *y*- dependence of the PSh amplitude are not independent. Nevertheless, as they are small values we can take the combined *x*- and *y*-correction as the product $\delta_{(x)}\delta_{(y)}$ of the individual correction coefficients.

In the *x*- and *y*-dependence fit (1) and (4) the free parameter values are practically the same $a_x \approx a_y$. Therefore, to apply for simultaneous correction $\delta_{(x)}$ and $\delta_{(y)}$ it is necessary to do normalization just once, say to a_x value. Therefore $a_y=1$, and the $\delta_{(y)}$ correction (5) will be

$$\delta_{(y)} = \frac{1}{A^{fit}_{(y)}} = \frac{1}{1 + b_y y + c_y y^2 + d_y y^3 + e_y y^4} \tag{7}$$

Now, the xy-corrected amplitude $A^{cor}_{(x,y)}$ is given by *y*-correction (7) of the x-corrected amplitude (3), that is

$$A^{cor}_{(x,y)} = \delta_{(x)}\delta_{(y)}A^{raw}_{(x,y)} = \frac{a_x}{A^{fit}_{(y)}A^{fit}_{(x)}}A^{raw}_{(x,y)} \tag{8}$$

The results are presented in **Figure 20**, with the xy-corrected amplitude $A^{cor}_{(x,y)}$, both for uncorrected (cut-ped) and corrected raw data.

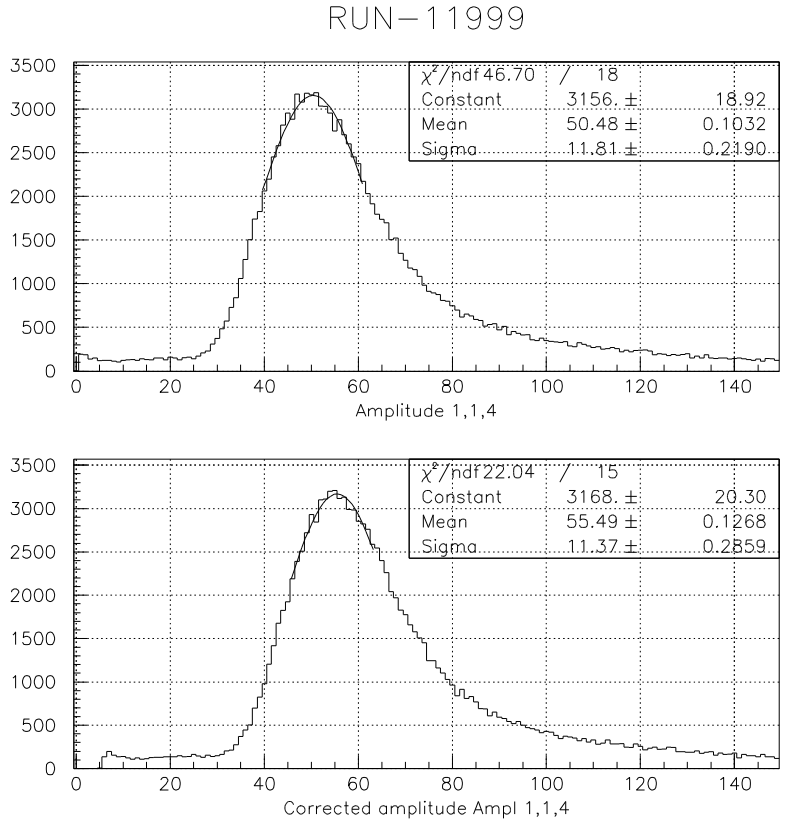

Figure 20. The *xy*-corrected amplitude of the raw pion amplitude distribution, initially presented in **Figure 7**, for slab (1,1,4)

The *xy*-corrected amplitude distributions for each slab arm 1, run 11999, are presented in **Figure 21**. For all runs the *xy*-corrected amplitude data are presented in **Figure 22**.

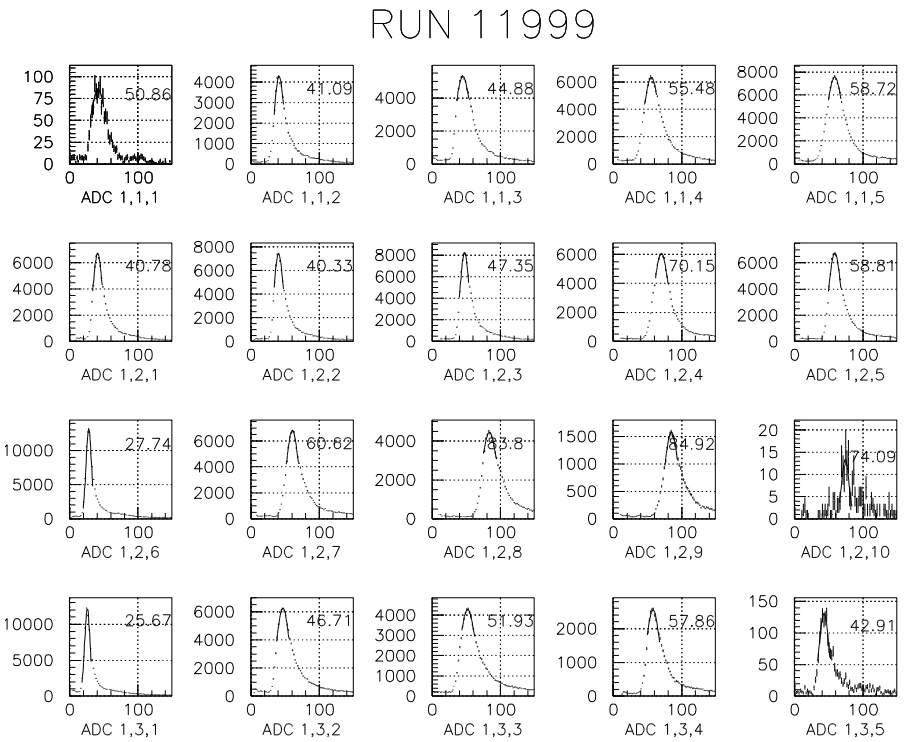

Figure 21. *xy*-corrected amplitude distributions for slabs arm 1, run 11999.

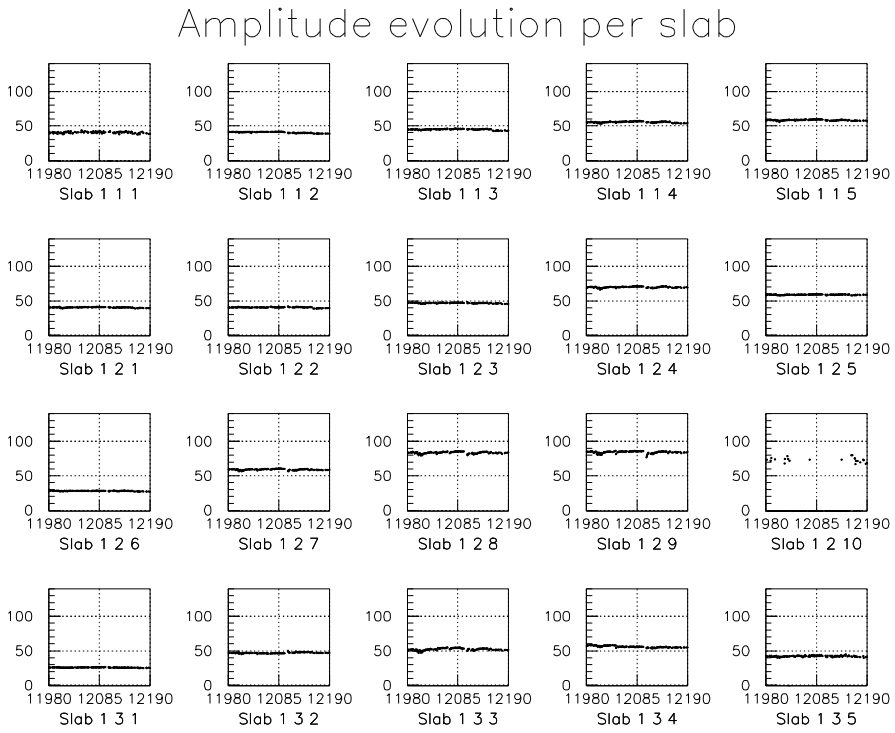

Figure 22. *xy*-corrected amplitude values for all slabs arm 1 and all runs.

To correct the dispersion in the 40 channel amplification values, and to obtain the same amplitude peak position (~100) for all slabs for the run 11999 for example, the first 20 amplitude values presented in **Figure 21** must be multiplied by the factor $\delta = \frac{100}{A^{cor}_{(x,y)}}$ presented in **Table 3**.

Table 3. The correction δ of the channel amplification inhomogeneity uses the following factors to obtain the same pion peak position (~100) for all slabs arm 1, run 11999 as in **Figure 21**.

1.962	2.462	2.292	1.824	1.689
2.452	2.500	2.105	1.420	1.739
3.930	1.649	1.186	1.174	1.298
3.836	2.173	1.950	1.670	2.489

5. Conclusions

In the present paper it was studied the Preshower detector amplitude signals produced by large scintillation slabs. They are affected by incident particle coordinate point (*x*,*y*) on the slab surface. It was studied the *x*- and *y*-dependence of the amplitude signal and the corresponding corrections has been applied. The final correction refers to the alignment of all 40 Preshower slab signals to one amplitude value. Now the electron rejection can be done with one and the same cut value on the amplitude spectra for all the 40 Preshower slabs.

Acknowledgements

This work was supported by CERN, the Ministry of Education and Research of Romania, the Ministry of Education and Youth of the Czech Republic and the Ministry of Industry, Science and Technologies of the Russian Federation.

References

[1] M.Pentia, S.Constantinescu, M.Gugiu, "The new preshower detector for DIRAC-II setup: characteristics and performances, DIRAC-NOTE-2011-03 (2011).